Supplementary Information for

Atmospheric Fate of 4:2 Fluorotelomer Alcohol using an Oxidation Flow Reactor and Proton Transfer Reaction Time-of-Flight Mass Spectrometry

Alessia A. Colussi[1], Trevor C. VandenBoer[1], Cora J. Young[1], and John Liggio[2]

[1] *Department of Chemistry, York University, Toronto, ON, Canada*

[2] *Air Quality Research Division, Environment and Climate Change Canada, Toronto, ON, Canada*

Corresponding Authors: John Liggio (john.liggio@ec.gc.ca) and Cora Young (youngcj@yorku.ca)

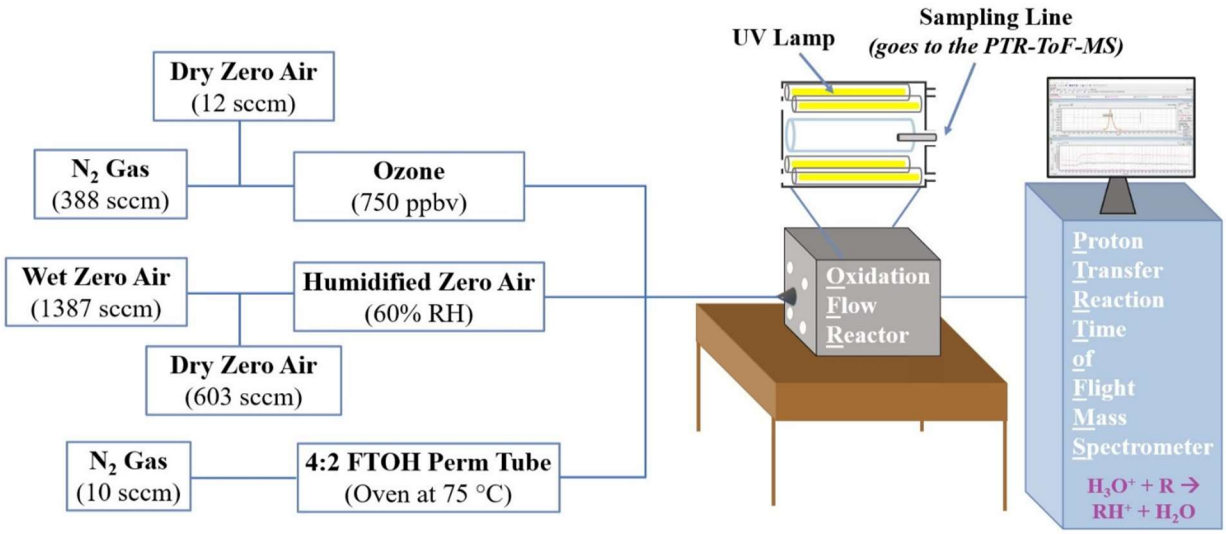

Figure S1. Simplified schematic of the experimental setup, e.g., at 60% RH, utilized in the described chamber experiments. Specific to the proposed research, UV light at 254 nm is provided by low-pressure mercury lamps to photolyze externally generated O_3. This photolysis produces $O(^1D)$ which then reacts with water vapour in the reactor (grey-outlined cylinder) to generate the necessary OH radicals. Approximately 10 mL min^{-1} N_2 is constantly flowing over a permeation device housing the liquid 4:2 FTOH. The N_2 flow containing permeated 4:2 FTOH will then meet a flow of humified zero air before combining with the O_3 flow. This total flow (O_3 + humified zero air + 4:2 FTOH) then enters a conical diffusion inlet leading into the OFR prior to passing into the PTR-ToF-MS.

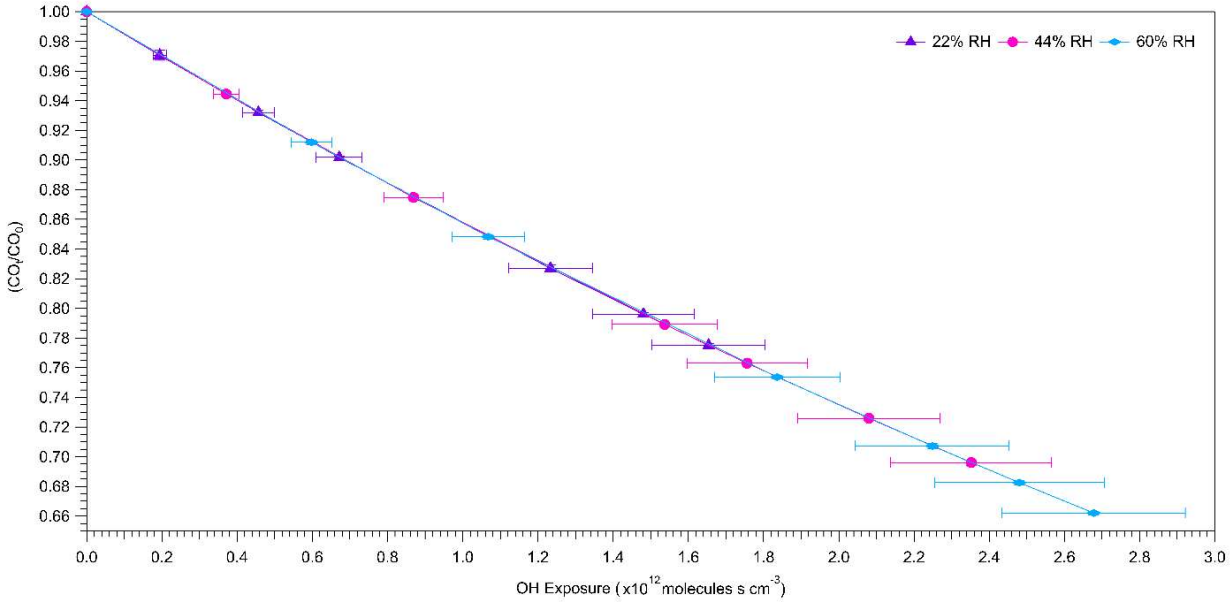

Figure S2. Offline calibrations were performed to measure the decay of CO with increasing OH exposure (molecules s cm^{-3}). Plotted against OH exposure is the ratio of $[CO]_0$, the initial CO concentration (parts-per-million-by-volume; 10^{-6} mol mol^{-1}, ppmv) without O_3 photolysis to generate OH (i.e., UV lamps were off; ~1.07 to 1.08 ppmv), and $[CO]_t$, the CO concentration in the presence of constant OH from O_3 (i.e., UV lamps were turned on).

Section S1. Determining OH Exposures at Different Relative Humidities

The OH exposure (molecules s cm^{-3}), which is the product of OH concentration (molecules cm^{-3}) and residence time (s) in the OFR, was determined by measuring the loss of CO as a function of time with respect to OH concentration (Figure S2; EQ S1).

$$\text{OH exposure} = -\left(\frac{1}{k_{CO}}\right) \ln \frac{[CO]_t}{[CO]_0} \qquad \textbf{(EQ S1)}$$

Here k_{CO} is the second-order rate constant at 298 K ((1.54 ± 0.14) × 10^{-13} cm^3 $molecules^{-1}$ s^{-1})[1], $[CO]_0$ is the CO concentration without O_3 photolysis (i.e., UV lamps were off) to generate OH, and $[CO]_t$ is the CO concentration in the presence of constant OH from O_3 photolysis controlled by voltages applied when the UV lamps were turned on.[2] The reaction between CO and OH is bimolecular and corresponds to a second-order rate law:

$$\frac{\Delta[CO]}{\Delta t} = -k_{CO}[CO][OH] \qquad \textbf{(EQ S2)}$$

Within the OFR, OH is continuously being produced via the photolysis of externally generated O_3 and is assumed to be constant over the residence time. Thus, under this condition, the reaction follows pseudo-first-order kinetics with respect to CO. Therefore, EQ S2 can be rewritten as:

$$\frac{\Delta[CO]}{\Delta t} = -k'[CO] \qquad \textbf{(EQ S3)}$$

then with respect to the conduct of an experiment over a given observation time for CO as:

$$\frac{\Delta[CO]_t}{[CO]_0} = -k'\Delta t \qquad \textbf{(EQ S4)}$$

Here, the OH exposure is defined as the time integrated OH concentration:

$$\text{OH exposure} = [OH]\Delta t \qquad \textbf{(EQ S5)}$$

Substituting EQ S5 into EQ S4 and rearranging to obtain an expression for OH exposure yields EQ S1.

The errors of the $\ln\left(\frac{[CO]_t}{[CO]_0}\right)$ term (EQ S6) and of the OH exposure (EQ S7) were determined to assess the precision of the kinetic method.

$$\frac{Sy}{y} = \sqrt{\left(\frac{[CO]_0\, error}{[CO]_0}\right)^2 + \left(\frac{[CO]_t}{[CO]_t}\right)^2} \qquad \textbf{(EQ S6)}$$

$$\frac{Sy}{y} = \sqrt{\left(\frac{k_{CO}\, error}{k_{CO}}\right)^2 + \left(\frac{ln\left(\frac{[CO]_t}{[CO]_0}\right) error}{ln\left(\frac{[CO]_t}{[CO]_0}\right)}\right)^2} \qquad \textbf{(EQ S7)}$$

Table S1. The OH exposure ranges and corresponding atmospheric photochemical ages when assuming a global average tropospheric OH concentration of 1.50×10^6 molecules cm^{-3}.[3]

Relative Humidity	OH Exposure Ranges (molecules s cm^{-3})	Photochemical Age Range (days)
22%	1.94×10^{11} to 1.65×10^{12}	1.50 to 12.76
44%	3.71×10^{11} to 2.35×10^{12}	2.86 to 18.15
60%	5.98×10^{11} to 2.68×10^{12}	4.61 to 20.66

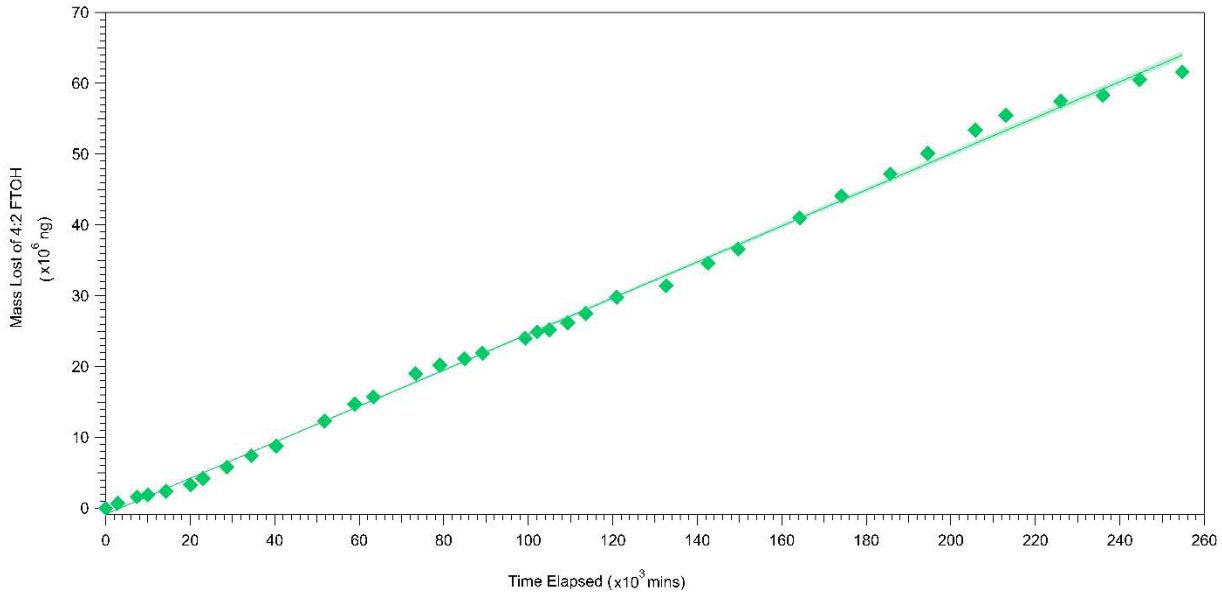

Figure S3. Gas-phase 4:2 FTOH was generated using a temperature-controlled (75°C), custom-made permeation device. Plotted here is the mass of 4:2 FTOH lost (ng) over a 26-week period. The permeation device's emission rate was determined as 254 ± 2 ng min^{-1} with a R^2 value of 0.9977 and a relative standard deviation, indicated by the green shading over each marker, of ± 0.8291%.

Section S2. Calibrating the PTR-ToF-MS for 4:2 FTOH

Assuming standard temperature and pressure, the following equations were used to calculate the 4:2 FTOH mixing ratios (EQ S8; ppbv), and their respective errors (EQ S9), on the calibration curves:

$$[4{:}\,2\ \mathrm{FTOH}] = y = (E_{4:2\ \mathrm{FTOH}})(Q_{4:2\ \mathrm{FTOH}})(MW_{4:2\ \mathrm{FTOH}})(V_m)(1 \times 10^9 \mathrm{ppbv}) \quad \textbf{(EQ S8)}$$

$$\frac{Sy}{y} = \sqrt{\left(\frac{E_{4:2\ \mathrm{FTOH}}\ \mathrm{error}}{E_{4:2\ \mathrm{FTOH}}}\right)^2 + \left(\frac{\sqrt{(Q_{N_2}\ \mathrm{error})^2 + (Q_{ZA}\ \mathrm{error})^2}}{(Q_{N_2}\ \mathrm{error} + Q_{ZA})}\right)^2} \quad \textbf{(EQ S9)}$$

In EQ S8, $E_{4:2\ FTOH}$ is the emission rate (ng min^{-1}) of the gaseous 4:2 FTOH generated using a custom-made permeation device, $Q_{4:2\ FTOH}$ is the volumetric flow rate within the OFR (L min^{-1}) during each experiment, $MW_{4:2\ FTOH}$ is the molecular weight of the 4:2 FTOH (g mol^{-1}), and V_m is the molar volume of air (~22.4 L mol^{-1}). In EQ S9, Q_{N_2} and N_{ZA} are the volumetric flow rates of nitrogen gas and zero air maintained by their respective mass flow controllers (mL min^{-1}).

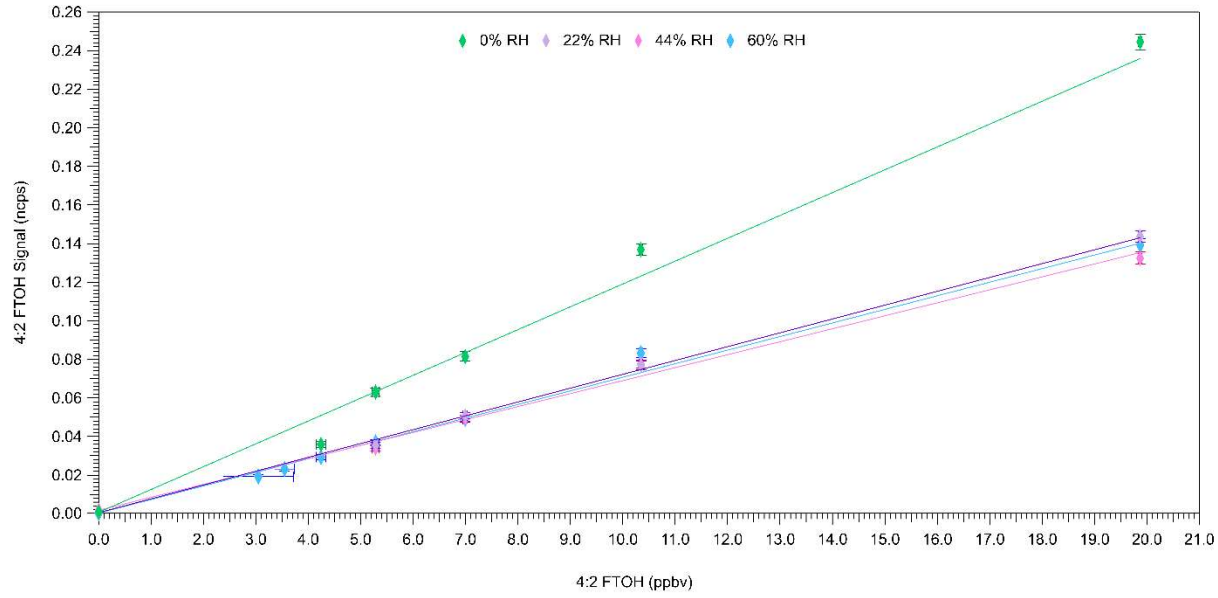

Figure S4. Calibration curves for the 4:2 FTOH at 0%, 22%, 44%, and 60% RH. Prior to starting the calibration, a dilution flow of zero air – containing no 4:2 FTOH – flowed through the system. Each RH had a R^2 greater than 0.99 and a minimum of three non-zero points. The y-axis depicts the blank corrected and normalized average signal of the 4:2 FTOH (ncps) and each calibration point's corresponding standard deviation. The x-axis shows the mixing ratio of 4:2 FTOH permeating off the PD (ppbv) and the propagated error at each calibration point.

Section S3. OFR: Assessing the Role of System Artifacts

To assess the impact of RH on the 4:2 FTOH + OH rate constants, three approaches were taken to determine the role of system artifacts. First, we ensured the flow within the OFR was laminar and calculated a Reynolds (Re; EQ S10 to S13) number of 16 indicative of this (i.e., Re < 2000) for an OFR residence time (τ) of 468 s and an OFR volume (V) of 0.016 m^3.

$$\boldsymbol{Re} = \frac{\rho u D}{\mu} \qquad \textbf{(EQ S10)}$$

$$\mathbf{u} = \frac{\mathrm{Q}}{\mathrm{A}} \qquad \textbf{(EQ S11)}$$

$$\mathbf{A} = \pi\left(\frac{D}{2}\right)^2 \qquad \textbf{(EQ S12)}$$

$$\mathbf{Q} = \frac{\mathrm{V}}{\tau} \qquad \textbf{(EQ S13)}$$

In EQs S10 to S13, ρ is the density of air assuming standard temperature and pressure (1.293 kg m^{-3}), μ is the dynamic viscosity of air (1.714 x 10^{-5} Pa s)[4], u is the flow velocity (1.06 x 10^{-3} m s^{-1}), D is the OFR diameter (I.D., 0.203 m), Q is the volumetric flow rate (m^3 s^{-1}), and A is the cross-sectional area (m^2). With laminar flow present in these experiments, the competition of diffusion driven wall losses relative to loss to OH was calculated using Fick's second law of diffusion (EQ S14). Here we provide a simplified estimate of the time (t) a molecule takes to diffuse (d) the length of the radius of the OFR (r). The 6.8 x 10^{-2} cm^2 s^{-1} diffusion coefficient of 1-hexanol[5] was used as a proxy for that of 4:2 FTOH.

$$\mathrm{t} = \frac{r^2}{4d} \qquad \textbf{(EQ S14)}$$

Since the diffusion coefficient of 1-hexanol is an upper limit for the diffusivity of 4:2 FTOH, it can take up to 417 s for 4:2 FTOH molecules to reach the OFR surface under our experimental conditions. Therefore, the loss of the 4:2 FTOH in our experiments may not result exclusively from reaction with OH and when the wall effects are assumed to be inconsequential the resulting first 'original' rate constants are obtained (Table S2). System effects, including those of the inlet and reactor surfaces, were then assessed by applying single and double exponential fitting functions to the calibration and 4:2 FTOH decay curves from OH oxidation using Igor Pro

(WaveMetrics®; Portland, OR, USA). Using each exponential fit, the plateaus at the conclusion of each OH exposure/decay period were compared to the originally determined rates.

This was done for both the calibration curves (Table S2) and 4:2 FTOH + OH experiments (Table S3) at each RH to compare and quantify the potential for system artifacts impacting our experimental observations. Within the calibrations, we found no evidence of surface effects, as the determined slopes were the same within error at each RH for each of the three fitting methods. Between the different RHs, changes in instrument response were observed – where the response was lower at 44% and 60% RH relative to 22% RH, yet within 10% of one another. All three responses were substantially lower than that determined under dry conditions.

For the oxidation experiments, the three different k_{obs} values for each RH are within the same order of magnitude and within 5 to 25% of one another. The single and double exponential fits result in different rate determinations in the oxidation experiments (Table S3), compared to the original assumption that no wall effects exist in the system. We believe that system artifacts may play a role in the slower k_{obs} at higher RH, and that RH does alter the PTR-ToF-MS sensitivity and likely affects the rate of reaction between 4:2 FTOH and OH radicals. Further study into the effects of RH on FTOH reaction rates with OH is necessary on systems with potential surface and instrumentation effects minimized.

Table S2. Comparing the original humified calibration curve data (Figure S4) to the data after being fit to single and double exponential functions.

22% RH			
	Original	**Single Exponential Fit**	**Double Exponential Fit**
R^2	0.9989	0.9992	0.9992
a (intercept)	$(-3.21 \pm 14.8) \times 10^{-4}$	$(-5.86 \pm 12.5) \times 10^{-4}$	$(-5.92 \pm 12.6) \times 10^{-4}$
b (slope)	$(7.27 \pm 0.14) \times 10^{-3}$	$(7.25 \pm 0.12) \times 10^{-3}$	$(7.26 \pm 0.12) \times 10^{-3}$
44% RH			
	Original	**Single Exponential Fit**	**Double Exponential Fit**
R^2	0.9941	0.9961	0.9964
a (intercept)	$(2.39 \pm 3.20) \times 10^{-3}$	$(1.91 \pm 2.59) \times 10^{-3}$	$(1.83 \pm 2.49) \times 10^{-3}$
b (slope)	$(6.66 \pm 0.30) \times 10^{-3}$	$(6.65 \pm 0.24) \times 10^{-3}$	$(6.65 \pm 0.23) \times 10^{-3}$
60% RH			
	Original	**Single Exponential Fit**	**Double Exponential Fit**
R^2	0.9922	0.9990	0.9993
a (intercept)	$(-4.21 \pm 2.29) \times 10^{-4}$	$(-5.71 \pm 9.20) \times 10^{-4}$	$(-6.72 \pm 7.95) \times 10^{-4}$
b (slope)	$(7.20 \pm 0.26) \times 10^{-3}$	$(7.07 \pm 0.10) \times 10^{-3}$	$(7.06 \pm 0.08) \times 10^{-3}$

Table S3. Comparing the original humified k_{obs} (Figure 3) to the data after being fit to single and double exponential functions.

22% Relative Humidity			
	Original	**Single Exponential Fit**	**Double Exponential Fit**
R^2	0.9772	0.9673	0.9756
a (intercept)	$(-1.71 \pm 0.87) \times 10^{-1}$	$(-1.97 \pm 0.98) \times 10^{-1}$	$(-1.77 \pm 0.86) \times 10^{-1}$
-b (-slope)	$(1.0 \pm 0.1) \times 10^{-12}$	$(9.8 \pm 0.9) \times 10^{-13}$	$(9.9 \pm 0.8) \times 10^{-13}$
44% Relative Humidity			
	Original	**Single Exponential Fit**	**Double Exponential Fit**
R^2	0.9843	0.9690	0.9720
a (intercept)	$(-3.50 \pm 0.67) \times 10^{-1}$	$(-3.65 \pm 1.10) \times 10^{-1}$	$(-2.91 \pm 1.14) \times 10^{-1}$
-b (-slope)	$(6.5 \pm 0.4) \times 10^{-13}$	$(7.5 \pm 0.7) \times 10^{-13}$	$(8.1 \pm 0.7) \times 10^{-13}$
60% Relative Humidity			
	Original	**Single Exponential Fit**	**Double Exponential Fit**
R^2	0.9982	0.9866	0.9816
a (intercept)	$(-3.93 \pm 0.27) \times 10^{-1}$	$(-4.69 \pm 0.85) \times 10^{-1}$	$(-4.18 \pm 1.07) \times 10^{-1}$
-b (-slope)	$(6.3 \pm 0.1) \times 10^{-13}$	$(7.4 \pm 0.4) \times 10^{-13}$	$(7.9 \pm 0.5) \times 10^{-13}$

Section S4. Comparing Gas-phase FTOH Measurements

While I-CIMS has been previously used for the identification of volatile PFAS in a laboratory setting[6-8], PTR-MS has many advantages over the conventional CIMS technique. For example, the generation of reagent ions within the PTR and the subsequent ionization of VOCs are spatially separated and individually controlled processes. While CIMS allows for more user control, the fixed PTR-MS conditions result in constant and well-defined settings in the drift tube and thus, makes the determination of absolute concentrations easier. Additionally, in the case of I-CIMS, water vapour plays an important role in the ionization efficiency of the iodide-adduct which ultimately influences instrument sensitivity.[9-12] The ionization of organic acids using I-CIMS has been shown to exhibit a strong dependence on RH.[13] Careful calibration of an I-CIMS as a function of the ion-molecule reactor water vapour pressure is necessary to map the instrument sensitivity for a given analyte to its quantity. In this work, the PTR sensitivity for the 4:2 FTOH appeared to decrease with increasing RH (Table S4). This was expected as PTR-MS sensitivities are known to be sample RH-dependent for some VOCs.[14] If the drift tube electric field is kept low to reduce fragmentation of analyte ions, a fraction of H_3O^+ can be converted to $H_3O^+(H_2O)$ and instrument sensitivity decreases with increasing humidity.

Table S4. Comparing the 4:2 FTOH sensitivities and two-second LODs determined for this work against measurements made by an I-CIMS.

	This Study			I-CIMS			
RH (%)	**R^2**	**Sensitivity (ncps $ppbv^{-1}$)**	**LOD (2 s, pptv)**	**Sensitivity (ncps $ppbv^{-1}$)[6]**	**LOD (3 s, pptv)[6]**	**Sensitivity (ncps $ppbv^{-1}$)[8]**	**LOD (3.33 s, pptv)[8]**
0	0.9913	$(12.7 \pm 0.6) \times 10^{-3}$	63	$(3.0 \pm 0.7) \times 10^{-3}$	7.9	2.0 ± 0.2	2.9
22	0.9989	$(7.3 \pm 0.1) \times 10^{-3}$	74				
44	0.9941	$(6.7 \pm 0.3) \times 10^{-3}$	200				
60	0.9922	$(7.2 \pm 0.3) \times 10^{-3}$	54				

Table S5. Comparing the sensitivity and two-second LOD determined for this work against those associated with VOC measurements made by a Vocus PTR-ToF-MS and a traditional PTR-ToF-MS. The one-second pptv LODs were calculated as(reported LOD) × [(1/(sqrt(1 s/reported time in s))].

	Vocus PTR-ToF-MS			**PTR-ToF-MS**		
Analyte	**Sensitivity (ncps ppbv^{-1})**	**Reported LOD (pptv, time)**	**LOD (pptv, 1 s)**	**Sensitivity (ncps ppbv^{-1})**	**Reported LOD (pptv, time)**	**LOD (pptv, 1 s)**
4:2 FTOH (this study)				$(12.7 \pm 0.6) \times 10^{-3}$	63 (2 s)	89
Acetone	5000 ± 700[15] 18400 ± 700[16]	14 (5 s)[15] 10 (1 s)[16]	31.3 10	30.9[17]	18 (60 s)[17]	139.4
Ethanol	80 ± 60[15]	90 (5 s)[15]	201.2	99.23[18]	-[18]	-

Table S6. Average urban air concentration (pg m^{-3}) of FTOHs in North America reported in the literature (∑gaseous and particulate phase) as parts-per-quadrillion by volume (10^{-15} mol mol^{-1}, ppqv).

	Martin et al., 2002 (~ 21.1 °C)[19]		**Shoeib et al., 2006** (~ 1.0 °C)[20]		**Ahrens et al., 2011** – ref. site 12 (~ 22.0 °C)[21]	
Analyte	pg m^{-3}	ppqv	pg m^{-3}	ppqv	pg m^{-3}	ppqv
6:2 FTOH	87	5.77	18	1.11	90	5.99
8:2 FTOH	55	2.86	41	1.99	144	7.51
10:2 FTOH	29	1.24	22	0.88	70	3.01

Table S7. Absorption cross-sections in the 230 to 350 nm region at 297 K[22] and 298 K.[23] In comparing the cross sections of the 1:2 and 6:2 FTALs at different wavelengths, we can infer that – due to the smaller absorption cross sections – less photolysis is occurring at the shorter wavelength. This suggests that the photolysis of 4:2 FTAL is just as likely to occur at 254 nm in the same manner as it would in the environment (loss of -COH to form a polyfluorinated radical) but would result in decreased 4:2 FTCA yields within the OFR.

	Absorption Cross-section (x 10^{-20} cm^2 $molecule^{-1}$)		
	298 K	297 K	
UV Wavelength (nm)	**1:2 FTAL (CF_3CH_2CHO)**	**1:2 FTAL (CF_3CH_2CHO)**	**6:2 FTAL ($C_6F_{13}CH_2CHO$)**
230	0.272	0.250	0.683
240	0.377	0.320	0.418
250	0.728	0.640	1.662
254	0.963	0.840	2.305
260	1.403	1.280	4.050
270	2.223	2.070	7.327
280	3.071	2.950	10.562
290	3.685	3.540	13.121
300	3.753	3.540	13.555
310	3.133	2.960	11.739
320	1.916	1.780	8.234
330	0.757	0.670	4.077
340	0.277	0.230	1.973
350	0.067	0.017	1.175

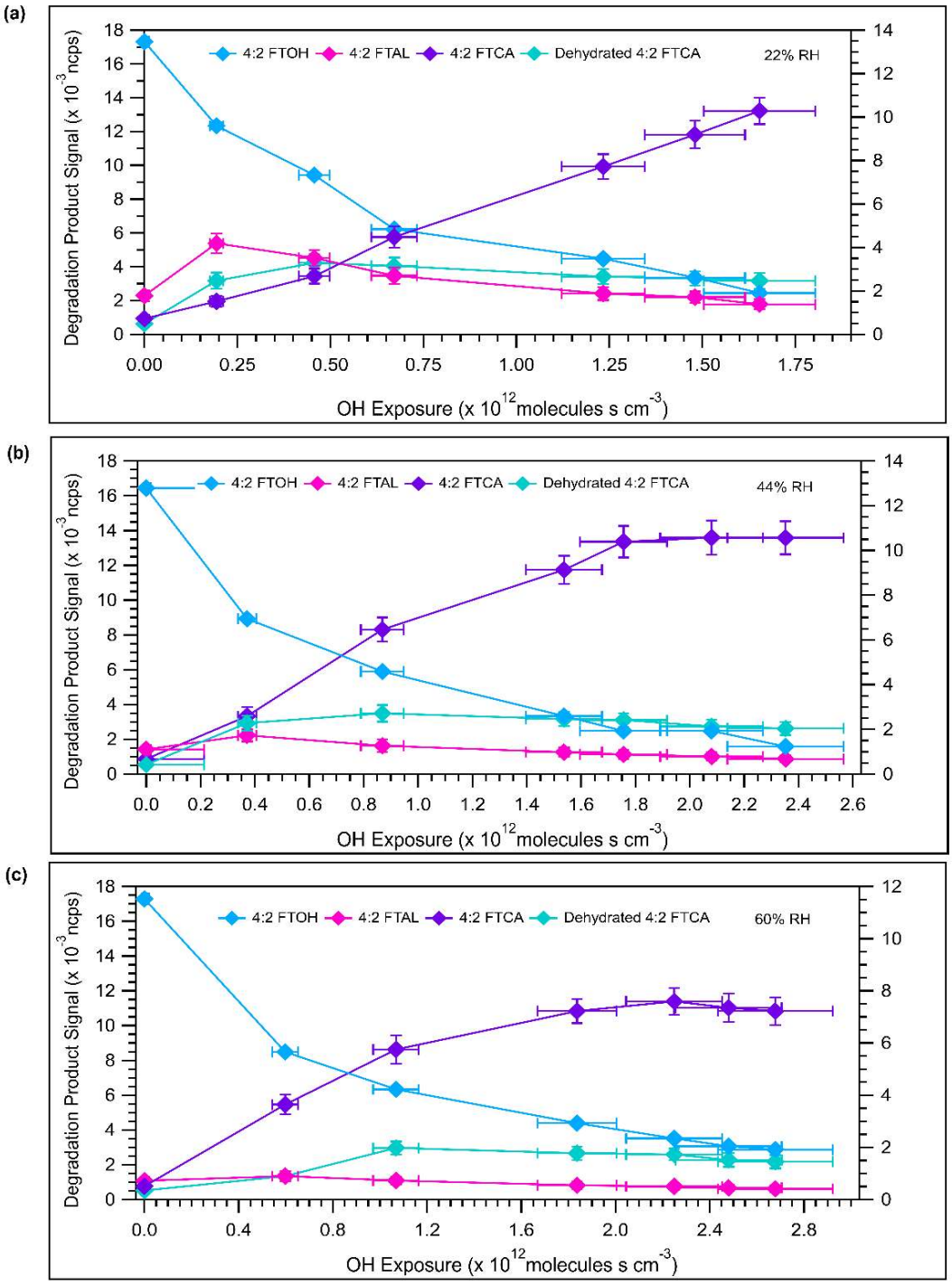

Figure S5. The change in 4:2 FTOH (m/z 265.027492), the detected degradation products (4:2 FTAL, m/z 263.011842; 4:2 FTCA, m/z 279.006757), and the suspected dehydrated 4:2 FTCA (m/z 260.996192) with increasing OH at **(a)** 22%, **(b)** 44%, and **(c)** 60% RH. The right y-axis depicts the 4:2 FTOH mixing ratio of permeating 4:2 FTOH (ppbv), and the propagated error at each point, as it reacts with OH radicals. On the left y-axis are the normalized average signals of the degradation products (ncps), with each point's corresponding standard deviation. The x-axis shows the OH exposure (molecules s cm^{-3}) and the propagated error at each point.

References

1. Liu, Y.; Sander, S. P. Rate Constant for the OH + CO Reaction at Low Temperatures. J. Phys. Chem. A 2015, 119 (39), 10060–10066.

2. Liu Q, Liggio J, Wentzell J, Lee P, Li K, Li SM. Atmospheric OH oxidation chemistry of particulate liquid crystal monomers: an emerging persistent organic pollutant in air. Environmental Science & Technology Letters. 2020 Jul 16;7(9):646-52.

3. Mao J, Ren X, Brune WH, Olson JR, Crawford JH, Fried A, Huey LG, Cohen RC, Heikes B, Singh HB, Blake DR. Airborne measurement of OH reactivity during INTEX-B. Atmospheric Chemistry and Physics. 2009 Jan 12;9(1):163-73.

4. Massman WJ. Molecular diffusivities of Hg vapor in air, O2 and N2 near STP and the kinematic viscosity and thermal diffusivity of air near STP. Atmospheric environment. 1999 Feb 1;33(3):453-7.

5. Tang, M.J., Shiraiwa, M., Pöschl, U., Cox, R.A. and Kalberer, M., 2015. Compilation and evaluation of gas phase diffusion coefficients of reactive trace gases in the atmosphere: Volume 2. Diffusivities of organic compounds, pressure-normalised mean free paths, and average Knudsen numbers for gas uptake calculations. *Atmospheric Chemistry and Physics*, pp.5585-5598.

6. Riedel, T. P.; Lang, J. R.; Strynar, M. J.; Lindstrom, A. B.; Offenberg, J. H. Gas-Phase Detection of Fluorotelomer Alcohols and Other Oxygenated Per- and Polyfluoroalkyl Substances by Chemical Ionization Mass Spectrometry. Environ. Sci. Technol. Lett. 2019, 6 (5), 289–293.

7. Bowers BB, Thornton JA, Sullivan RC. Evaluation of iodide chemical ionization mass spectrometry for gas and aerosol-phase per-and polyfluoroalkyl substances (PFAS) analysis. Environmental Science: Processes & Impacts. 2023 Feb 22;25(2):277-87.

8. Mattila, J. M.; Offenberg, J. H. Measuring Short-Chain per- and Polyfluoroalkyl Substances in Central New Jersey Air Using Chemical Ionization Mass Spectrometry. Journal of the Air & Waste Management Association 2024, 74 (8), 531–539. https://doi.org/10.1080/10962247.2024.2366491.

9. Huey LG, Hanson DR, Howard CJ. Reactions of SF6-and I-with atmospheric trace gases. The Journal of Physical Chemistry. 1995 Apr;99(14):5001-8.

10. Slusher DL, Huey LG, Tanner DJ, Flocke FM, Roberts JM. A thermal dissociation–chemical ionization mass spectrometry (TD-CIMS) technique for the simultaneous measurement of peroxyacyl nitrates and dinitrogen pentoxide. Journal of Geophysical Research: Atmospheres. 2004 Oct 16;109(D19).

11. Lee BH, Lopez-Hilfiker FD, Mohr C, Kurtén T, Worsnop DR, Thornton JA. An iodide-adduct high-resolution time-of-flight chemical-ionization mass spectrometer: Application to atmospheric inorganic and organic compounds. Environmental science & technology. 2014 Jun 3;48(11):6309-17.

12. Lopez-Hilfiker FD, Iyer S, Mohr C, Lee BH, D'Ambro EL, Kurtén T, Thornton JA. Constraining the sensitivity of iodide adduct chemical ionization mass spectrometry to multifunctional organic molecules using the collision limit and thermodynamic stability of iodide ion adducts. Atmospheric Measurement Techniques. 2016 Apr 6;9(4):1505-12.

13. Brophy P, Farmer DK. A switchable reagent ion high resolution time-of-flight chemical ionization mass spectrometer for real-time measurement of gas phase oxidized species: characterization from the 2013 southern oxidant and aerosol study. Atmospheric Measurement Techniques. 2015 Jul 22;8(7):2945-59.

14. Ernle L, Wang N, Bekö G, Morrison G, Wargocki P, Weschler CJ, Williams J. Assessment of aldehyde contributions to PTR-MS m/z 69.07 in indoor air measurements. Environmental Science: Atmospheres. 2023;3(9):1286-95.

15. Jensen AR, Koss AR, Hales RB, de Gouw JA. Measurements of volatile organic compounds in ambient air by gas-chromatography and real-time Vocus PTR-TOF-MS: calibrations, instrument background corrections, and introducing a PTR Data Toolkit. Atmospheric Measurement Techniques. 2023 Nov 8;16(21):5261-85.

16. Krechmer J, Lopez-Hilfiker F, Koss A, Hutterli M, Stoermer C, Deming B, Kimmel J, Warneke C, Holzinger R, Jayne J, Worsnop D. Evaluation of a new reagent-ion source and focusing ion–molecule reactor for use in proton-transfer-reaction mass spectrometry. Analytical chemistry. 2018 Sep 17;90(20):12011-8.

17. Lee AK, Abbatt JP, Leaitch WR, Li SM, Sjostedt SJ, Wentzell JJ, Liggio J, Macdonald AM. Substantial secondary organic aerosol formation in a coniferous forest: observations of both day-and nighttime chemistry. Atmospheric Chemistry and Physics. 2016 Jun 3;16(11):6721-33.

18. Wu C, Wang C, Wang S, Wang W, Yuan B, Qi J, Wang B, Wang H, Wang C, Song W, Wang X. Measurement report: Important contributions of oxygenated compounds to emissions and chemistry of volatile organic compounds in urban air. Atmospheric Chemistry and Physics. 2020 Dec 2;20(23):14769-85.

19. Martin JW, Muir DC, Moody CA, Ellis DA, Kwan WC, Solomon KR, Mabury SA. Collection of airborne fluorinated organics and analysis by gas chromatography/chemical ionization mass spectrometry. Analytical Chemistry. 2002 Feb 1;74(3):584-90.

20. Shoeib M, Harner T, Vlahos P. Perfluorinated chemicals in the Arctic atmosphere. Environmental science & technology. 2006 Dec 15;40(24):7577-83.

21. Ahrens L, Shoeib M, Harner T, Lee SC, Guo R, Reiner EJ. Wastewater treatment plant and landfills as sources of polyfluoroalkyl compounds to the atmosphere. Environmental science & technology. 2011 Oct 1;45(19):8098-105.

22. Chiappero MS, Malanca FE, Argüello GA, Wooldridge ST, Hurley MD, Ball JC, Wallington TJ, Waterland RL, Buck RC. Atmospheric chemistry of perfluoroaldehydes (C x F2 x+ 1CHO) and fluorotelomer aldehydes (C x F2 x+ 1CH2CHO): quantification of the important role of photolysis. The Journal of Physical Chemistry A. 2006 Nov 2;110(43):11944-53.

23. Sellevåg SR, Kelly T, Sidebottom H, Nielsen CJ. A study of the IR and UV-Vis absorption cross-sections, photolysis and OH-initiated oxidation of CF 3 CHO and CF 3 CH 2 CHO. Physical Chemistry Chemical Physics. 2004;6(6):1243-52.